Polarization enhancement and suppression of four-wave mixing in multi-Zeeman levels

Zhiguo Wang (王志国), Yuxin Fu (付雨欣), Yue Song (宋 悦), Guoxian Dai (代国宪), Feng Wen (闻 峰), Jinyan Zhao (赵金燕), and Yanpeng Zhang (张彦鹏)*

Key Laboratory for Physical Electronics and Devices, Ministry of Education, Shanxi Key Laboratory of Information Photonic Technique, Xi'an Jiaotong University, Xi'an 710049, China

**Corresponding author: ypzhang@mail.xjtu.edu.cn.*

Received September 26, 2010; accepted January 28, 2011; posted online May 26, 2011

Polarization dependence of the enhancement and suppression of four-wave mixing (FWM) in a multi-Zeeman level atomic system is investigated both theoretically and experimentally. A dressing field applied to the adjacent transition can cause energy level splitting. Therefore, it can control the enhancement and suppression of the FWM processes in the system due to the effect of electromagnetically induced transparency. The results show that the pumping beams with different polarizations select the transitions between different Zeeman levels that, in turn, affect the enhancement and suppression efficiencies of FWM.

OCIS codes: 270.1670, 190.4180, 190.4223.
doi: 10.3788/COL201109.072701.

In the past few decades, various studies on multi-wave mixing (MWM) processes have been carried out[1−9]. Given that weak generated signals can be transmitted through the resonant atomic medium, effects related to electromagnetically induced transparency (EIT)[10] are considered excellent tools in investigating MWM processes. Furthermore, when multi-Zeeman energy levels are involved in the atomic systems[11,12] of EIT and four-wave mixing (FWM) processes[3,7,13,14], polarizations of the involved laser beams are expected to play a important role in these processes. EIT and FWM processes can be effectively controlled by selecting different transitions between various Zeeman sublevels through the adjustment of the polarization states of the involved laser beams[3,7,11−14]. Moreover, the FWM efficiencies in multi-level atomic systems can be modified by adding dressing laser beams.

In this letter, we aim to demonstrate experimentally that degenerate FWM (DFWM) is enhanced or suppressed by the combined polarization and dressing effects. The polarizations of pumping beams are changed to select the transitions between different Zeeman levels that usually have different transition strengths resulting from distinct Clebsch–Gordan (CG) coefficients[11,12]. In this process, the dressing beam determines the effective frequency detuning of the probe beam from multi-Zeeman levels. Compared with previous research[7], we have observed the different rules of enhancement and suppression of FWM as a result of selecting different transition passages. The experimental observations are explained by the interplay among multi-dressing fields and multi-transition passages.

We considered the FWM process in a ladder-type three-level atomic system (Fig. 1(a)). There are four laser beams applied to the system, including two pumping laser beams E_c (ω_c, k_c, and Rabi frequency $G_{c,M}$) and E_c' (ω_c, k_c', $G_{c,M}'$), a weak probe field E_p (ω_p, k_p, $G_{p,M}$), and a dressing field E_d (ω_d, k_d, $G_{d,M}$), where subscript M represent the magnetic quantum number of the lower states in transitions in which these fields were radiated. These pulse laser beams are aligned in the spatial configuration shown in Fig. 1(b). The two beams, E_c and E_c', have a small angle of 0.3° and are tuned to drive the transition $|a\rangle$ $(3S_{1/2})$ to $|b\rangle$ $(3P_{3/2})$. Generally, E_c propagates in the opposite direction of the probe field E_p. A population grating between states $|a\rangle$ and $|b\rangle$ induced by E_c and E_c' (both with frequency ω_c) is probed by beam E_p with the same frequency (ω_c). This interaction generates a DFWM signal E_f (Fig. 1(a)), which satisfies the phase-matching condition[14]: $k_f = k_p + k_c - k_c'$.

The experiment was carried out in sodium atoms placed in a heat pipe oven and involved three energy levels. The two pumping laser beams, E_c and E_c', and the

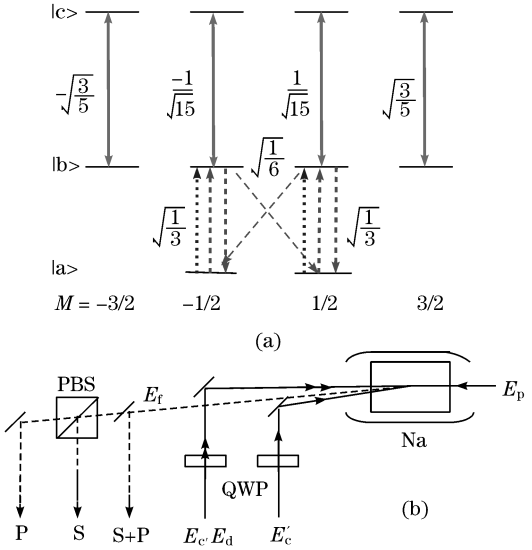

Fig. 1. (a) Zeeman structure of the three-level ladder-type atomic system generating the FWM signal E_f. Solid line: dressing field E_d; Short-dashed lines: the linearly polarized pumping fields E_c and E_c'; long-dashed lines: the circular-polarized pumping fields; dotted line: the probe field E_p; (b) schematic diagram of the experimental configuration.

weak probe field $E_{\rm p}$ were from the same near-transform-limited dye lasers (10-Hz repetition rate, 5-ns pulse-width and 0.04-cm^{-1} linewidth), while laser $E_{\rm d}$ was from another similar dye laser. As to the three former beams, the frequency detuning followed $\Delta_{\rm c} = \omega_{\rm ba} - \omega_{\rm c}$, where $\omega_{\rm ba}$ represented the resonance frequency between $|{\rm a}\rangle$ and $|{\rm b}\rangle$. The additional dressing field $E_{\rm d}$ was applied to the transition between $|{\rm b}\rangle$ and the third level $|{\rm c}\rangle$ ($4D_{3/2,5/2}$) with a frequency detuning $\Delta_{\rm d}$ ($= \omega_{\rm cb} - \omega_{\rm d}$). Two quarter-wave plates (QWPs) with a rotation angle θ were used to change the polarizations of the pumping fields $E_{\rm c}$ and $E'_{\rm c}$ that can be decomposed into linear- and circular-polarized components, respectively. The generated DFWM signal was split into two equal components using a 50% beam splitter before detection; one component was detected directly (denoted as $I^{\rm T}$), and the other was further decomposed into P- and S- polarized components using a polarized beam splitter (PBS), denoted as $I^{\rm P}$ and $I^{\rm S}$, respectively.

In the classical description to explain polarization dependence of FWM signals, the intensity of the FWM signal is proportional to the square of the atomic polarization induced in the medium. In terms of phase-conjugated FWM generation in the cascade atomic system at frequency $\omega_{\rm f} = \omega_{\rm c} - \omega_{\rm c} + \omega_{\rm p}$ (as shown in Fig. 1 with beam $E_{\rm d}$), the nonlinear polarization along i ($i = x$, y) direction is given by

$$P_i^{(3)}(\omega_{\rm s}) = \varepsilon_0 \sum_{jkl} \chi_{ijkl}^{(3)}\Big(\omega_{\rm f}; \omega_{\rm c}, -\omega_{\rm c}, \omega_{\rm p}\Big) E_{{\rm c}j}(\omega_{\rm c}) E'^{*}_{{\rm c}k}(\omega_{\rm c}) E_{{\rm p}l}(\omega_{\rm p}), \quad (1)$$

where $\chi_{ijkl}^{(3)}(\omega_{\rm f}; \omega_{\rm c}, -\omega_{\rm c}, \omega_{\rm p})$ is the tensor component of the third-order nonlinear susceptibility. Given the isotropic medium as Na atomic vapor, and considering that all the incident beams and signals are transverse waves, only four nonzero tensor elements are involved in this system: χ_{xxxx}, χ_{yxxy}, χ_{yyyx}, and χ_{yxyx}. Therefore there exist 16 transition pathways in the FWM generation[3].

We take the transition passage $\left|{\rm a}_{-1/2}\right\rangle \xrightarrow{G_{\rm c1}^0} \left|{\rm b}_{-1/2}\right\rangle \xrightarrow{(G_{\rm c2}'^{-})^*} \left|{\rm a}_{1/2}\right\rangle \xrightarrow{G_{\rm p2}^0} \left|{\rm b}_{1/2}\right\rangle \xrightarrow{(G_{\rm f1}^{+})^*} \left|{\rm a}_{-1/2}\right\rangle$ as an example to explain the transition process. The first step involves the ground state particle $\left|{\rm a}_{-1/2}\right\rangle$, which absorbs a coupling photon $G_{\rm c1}^0$ and transits to the dressed state $\left|{\rm b}_{-1/2}\right\rangle$, expressed as $\left|{\rm a}_{-1/2}\right\rangle \xrightarrow{G_{\rm c1}^0} \left|{\rm b}_{-1/2}\right\rangle$. In the second step, the particle emits a coupling photon $(G_{\rm c2}'^{-})^*$ and transits to the dressed state $\left|{\rm a}_{1/2}\right\rangle$, expressed as $\left|{\rm b}_{-1/2}\right\rangle \xrightarrow{(G_{\rm c2}^{-})^*} \left|{\rm a}_{1/2}\right\rangle$ in the transition passage. Third, the particle absorbs a probe photon $G_{\rm p2}^0$ and transits to the dressed state $\left|{\rm b}_{1/2}\right\rangle$, expressed as $\left|{\rm a}_{1/2}\right\rangle \xrightarrow{G_{\rm c1}^0} \left|{\rm b}_{1/2}\right\rangle$ in the transition passage. Fourth, the stimulated particle transits back to state $\left|{\rm a}_{-1/2}\right\rangle$ and emits a pumping photon $(G_{\rm f1}^{+})^*$, expressed as $\left|{\rm b}_{1/2}\right\rangle \xrightarrow{G_{\rm f1}^{+}} \left|{\rm b}_{-1/2}\right\rangle$.

To explain further, let us assume P polarization direction as the quantization axis, the component of the signal perpendicular to it (S polarization) can be decomposed into balanced left- and right-circularly-polarized parts, and the component parallel to it (P polarization) remains linearly polarized[7]. In the real experiment, we can express the detected intensities of $I^{\rm P}$, $I^{\rm S}$, and the total intensity $I^{\rm T}$ as $I^{\rm P} = I_{\rm L}\cos^2\alpha + I_{\rm C}/2$, $I^{\rm S} = I_{\rm L}\sin^2\alpha + I_{\rm C}/2$ and $I^{\rm T} = I^{\rm S} + I^{\rm P} = I_{\rm L} + I_{\rm C} I^{\rm T} = I^{\rm S} + I^{\rm P} = I_{\rm L} + I_{\rm C}$, respectively, where α is the angle between the P polarization and the direction of the linearly polarized signal, and $I_{\rm L}$ and $I_{\rm C}$ are the linearly and circularly polarized components contained in the generated FWM signals, respectively.

We can obtain the $\mathbf{E}_{\rm f}^{\rm P}$ intensity expression when changing the polarization of the pump field $E'_{\rm c}$, expressed as $\rho_{\rm ba}^{P} \propto \rho_{\rm ba}^{(3)}\sqrt{(\sin^4\theta + \cos^4\theta)}$, and when changing both the polarizations of $E_{\rm c}$ and $E'_{\rm c}$ expressed as $\rho_{\rm ba}^{P} \propto \rho_{\rm ba}^{(3)}\sqrt{\sin^4\theta + \cos^4\theta}\sqrt{\sin^4(\theta+\pi/4) + \cos^4(\theta+\pi/4)}$. In the latter expression, $\rho_{\rm ba}^{(3)} = -{\rm i}G_{\rm p}G_{\rm c}(G'_{\rm c})^*/F_2F_1^2$, where $F_1 = (\Gamma_{\rm ba} + {\rm i}\Delta_{\rm c}) + G_{\rm d}^2/d_1 + (G_{\rm c} + G'_{\rm c})^2/\Gamma_{\rm aa} + (G_{\rm c} + G'_{\rm c})^2/d_2$ and $F_2 = \Gamma_{\rm aa} + (G_{\rm c} + G'_{\rm c})^2/d_3$, with $d_1 = [\Gamma_{\rm aa} + {\rm i}(\Delta_{\rm c} + \Delta_{\rm d})]$, $d_2 = \Gamma_{\rm bb} + G_{\rm d}^2/(\Gamma_{\rm bc} - {\rm i}\Delta_{\rm d})$, and $d_3 = (\Gamma_{\rm ba} + {\rm i}\Delta_{\rm c}) + G_{\rm d}^2/[\Gamma_{\rm cb} + {\rm i}(\Delta_{\rm c} + \Delta_{\rm d})]$. In addition, $\pi/4$ is the polarization difference-angle between $E_{\rm c}$ and $E'_{\rm c}$. Similarly, the expression of $\mathbf{E}_{\rm f}^{\rm S}$ intensity when changing the polarization of $E'_{\rm c}$ is $\rho_{\rm ba}^{\rm S} \propto \rho_{\rm ba}^{(3)}\sqrt{\sin^2\theta\cos^2\theta}$. Meanwhile, the expressions of changing the polarizations of $E_{\rm c}$ and $E'_{\rm c}$ simultaneously is $\rho_{\rm ba}^{\rm S} \propto \rho_{\rm ba}^{(3)}\sqrt{(\sin^4\theta + \cos^4\theta)}\sqrt{\sin^2(\theta+\pi/4)\cos^2(\theta+\pi/4)}$.

The suppression and enhancement of the DFWM processes occur as the probe field is set under different frequency detuning conditions. For example, when $\Delta_{\rm c} = 0$, the DFWM signal is suppressed by the dressing field (Fig. 2). To understand clearly the influence of the incident beams on the suppression and enhancement of the FWM processes, we investigated the P and S polarization components of the signals separately. Meanwhile, the total intensity is the sum of intensities in these two polarization components (Figs. 2(a)−(c)). The background represents the signal strength of the pure DFWM with no dressing field. The peaks show that the signal has been enhanced, and the dips represent signal suppression with the dressing field at different polarizations of the pumping beam.

The background of the P polarization component of the FWM signal is high at $\theta = 0°$; when $\theta = 45°$, it reaches the lowest point, and then turns back to the original height when $\theta = 90°$ (Fig. 2(b)). The period $\pi/2$ of the background curve is determined by $\rho_{\rm ba}^{\rm P} \propto \rho_{\rm ba}^{(3)}\sqrt{(\sin^4\theta + \cos^4\theta)}$. Similarly, the trend of the background of the S direction FWM signal shown in Fig. 2(c) is highest at $\theta = 0°$; it then descends to the lowest point at $\theta = 45°$ and ascends to the original height at $\theta = 90°$, with the period $\pi/2$ obtained by $\rho_{\rm ba}^{\rm S} \propto \rho_{\rm ba}^{(3)}\sqrt{\sin^2\theta\cos^2\theta}$. Given that the trends of both P and S direction FWM signals are the same, the trend of the P+S direction FWM signal shown in Fig. 2(a) is also from high point to low point, after which it returns to the initial point.

When Δ_c is set small and the polarization of the E_c' field is changed by the QWP at 0°, the sub-systems generating FWM signal perturbation chains follow this passage: $\left|a_{-1/2}\right\rangle \xrightarrow{G_{c1}^0} \left|b_{-1/2}\right\rangle \xrightarrow{(G_{c1}'^0)^*} \left|a_{-1/2}\right\rangle \xrightarrow{G_p^0} \left|b_{-1/2}\right\rangle \xrightarrow{(G_f^0)^*} \left|a_{-1/2}\right\rangle$. The signal strength can be denoted by multiplying the CG coefficient of each transition, which is $(1/\sqrt{3})\times(1/\sqrt{3})\times(1/\sqrt{3})\times(1/\sqrt{3}) = 1/9$. When the polarization of the E_c' field is changed by the QWP at 45°, the sub-systems generating the FWM signal perturbation chains follow and is expressed as $\left|a_{-1/2}\right\rangle \xrightarrow{G_{c1}^0} \left|b_{-1/2}\right\rangle \xrightarrow{(G_{c2}'^-)^*} \left|a_{1/2}\right\rangle \xrightarrow{G_{p2}^0} \left|b_{1/2}\right\rangle \xrightarrow{(G_{f1}^+)^*} \left|a_{-1/2}\right\rangle$. Similarly, the multiplied CG coefficients of this passage is represented by $(1/\sqrt{3})\times(1/\sqrt{6})\times(1/\sqrt{6})\times(1/\sqrt{3}) = 1/18$. Thus, G_c is smaller at 45° than when it is at 0°, while G_d remains the same. Thus, the self-dressing efficiency at 45° is less than at 0°. Consequently, the depth of the suppression dip is relatively less at 45° than at 0°.

When E_p, E_c, and E_c' are far detuned, the DFWM is enhanced (Fig. 3). Similar to the background of the suppression curve, the background of both the P and S polarization components of the FWM signal in Fig. 3 is highest at $\theta = 0°$; it reaches its lowest point at $\theta = 45°$ before returning to the original height when $\theta = 90°$. However, the polarization dependence of the enhanced peak heights for the S polarization component in this case is different from that in the suppression, it descends as QWP is rotated from 0° to 45°. In a far detuning condition, this polarization variation of E_c enlarges α. According to $I^P = I_L^P + I_C/2 = I_L\cos^2\alpha + I_C/2$ and $I^S = I_L^S + I_C/2 = I_L\sin^2\alpha + I_C/2$, as we rotate the QWP

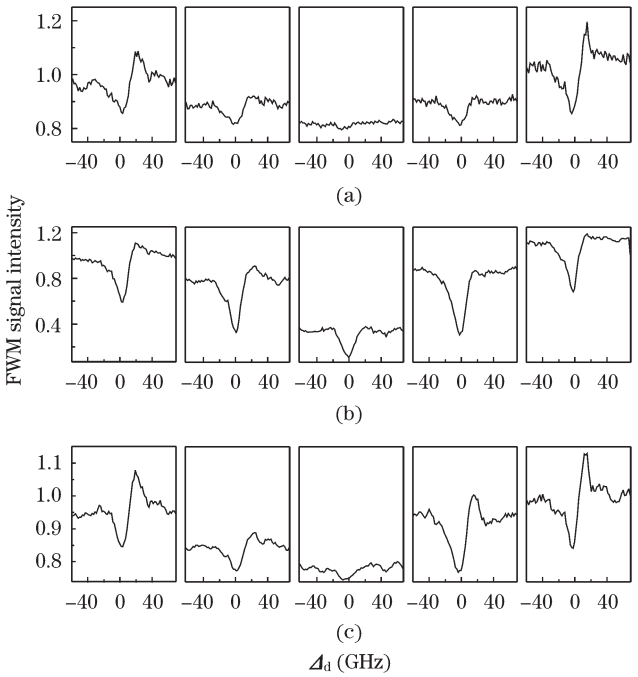

Fig. 2. E_c' polarization dependence of the suppressed DFWM signals. (a)−(b) variations of I^T, I^P, and I^S (by scanning Δ_d) versus rotation angle θ (0°, 20°, 45°, 70°, and 90°, from left to right), respectively. $\Delta_c = 0$, and the powers of the coupling fields E_c and E_c' are both 100 μW.

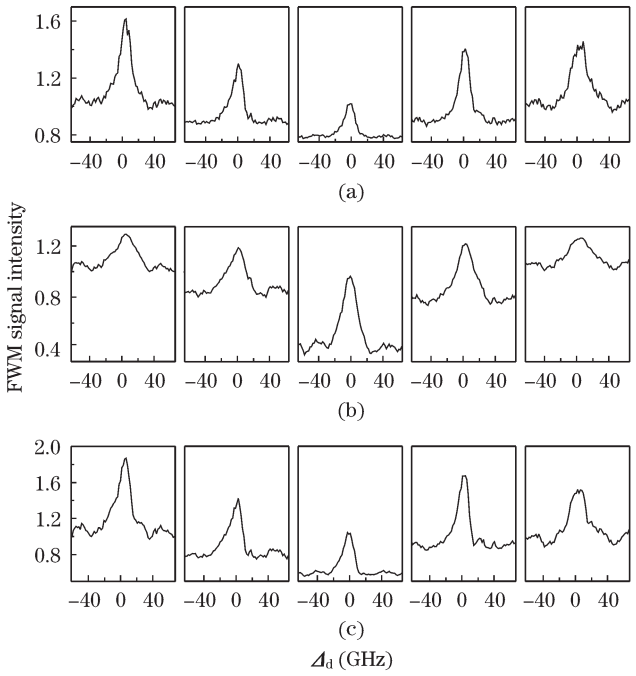

Fig. 3. E_c' polarization dependence of the enhanced DFWM signals. (a)−(c) variations of I^T, I^P, and I^S (by scanning Δ_d) versus rotation angle θ (0°, 20°, 45°, 70°, and 90°, from left to right), respectively. $\Delta_c = -67$ GHz, and the powers of the coupling fields E_c and E_c' are both 100 μW.

from 0° to 45°, the S polarized component projecting from the linearly polarized FWM decreases, while the P polarization component from the linearly polarized FWM increases. Given that the efficiency of the linearly polarized FWM is larger than that of the circularly polarized FWM, the dressing efficiency of the S polarization component is relatively reduced compared with the condition when E_c is circularly polarized; meanwhile, the P polarization component is relatively enhanced.

Now let us consider the condition of changing the polarizations of E_c and E_c' simultaneously. Figure 4(b) shows that the background of the P polarization FWM signal is highest at $\theta = 0°$. When $\theta = 22.5°$, it reaches the lowest point and then returns to the initial height when $\theta = 45°$. From $\rho_{ba}^P \propto \rho_{ba}^{(3)}\sqrt{\sin^4\theta + \cos^4\theta}\sqrt{\sin^4(\theta+\pi/4) + \cos^4(\theta+\pi/4)}$, we can see that the period of the background curve of the P polarization component is at $\pi/4$. Similarly, the background of the S polarization component shown in Fig. 4(c) is highest at $\theta = 0°$, descends to the lowest point at $\theta = 22.5°$, and ascends to the original height at $\theta = 45°$. This can be found in $\rho_{ba}^S \propto \rho_{ba}^{(3)}\sqrt{(\sin^4\theta + \cos^4\theta)}\sqrt{\sin^2(\theta+\pi/4)\cos^2(\theta+\pi/4)}$, the period of which is still at $\pi/4$. Given that the trends of both P and S polarization components of the FWM signal are similar, the trend of the P+S signal, namely the total FWM signal, is also from high point to low point and then back to the original point (Fig. 4(a)). Thus, the variation period is reduced to half of the cases with changing E_c only, that is, when two QWPs are used to change the polarizations of the E_c and E_c' beams simultaneously. Furthermore, the suppression peak

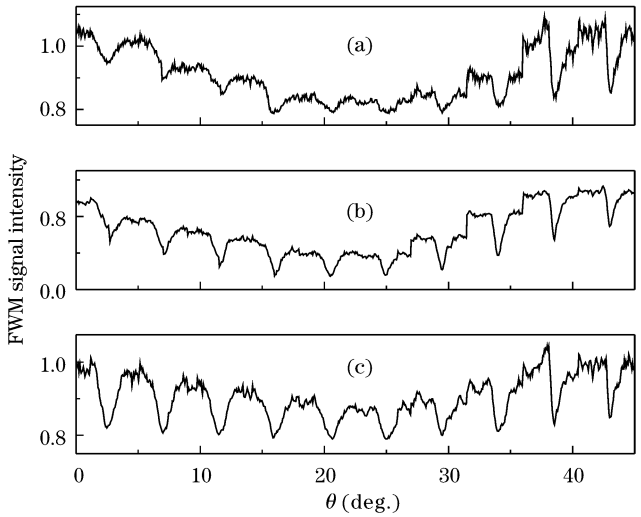

Fig. 4. E_c and E_c' polarization dependence of the suppressed DFWM signals. (a)−(c) variations of I^T, I^P, and I^S (by scanning Δ_d) versus rotation angle θ. $\Delta_c = 0$, and the powers of the coupling fields E_c and E_c' are both 100 μW.

approaches 0 at about $\theta = 22.5°$.

In conclusion, we report the relevant theoretical analyses regarding the evolutions of dressed DFWM effects versus the polarization states of the pumping fields. In the suppression case, the generated DFWM signals in P and S polarizations are both descending as the QWP rotates from 0° to 45°. This is caused by different dressing strengths for the linearly polarized and circularly polarized DFWM signals. In the enhancement case, as the QWP is rotated in the above interval, the dependence curve for the S-polarized DFWM signal decreases, while the P-polarization component increases.

This work was supported by the National Natural Science Foundation of China (Nos. 10974151, 61078002, and 61078020), the New Century Excellent Talent of Ministry of Education of China (No. 08-0431), and the Cross-Disciplinary Project of Xi'an Jiaotong University (Nos. 2009xjtujc08, XJJ20100100, and XJJ20100151).

References

1. Y. Wu and L. Deng, Phys. Rev. Lett. **93,** 143904 (2004).
2. Y. Wu, J. Saldana, and Y. F. Zhu, Phys. Rev. A **67,** 013811 (2003).
3. R. Wang, Y. Du, Y. Zhang, H. Zheng, Z. Nie, C. Li, Y. Li, J. Song, and M. Xiao, J. Opt. Soc. Am. B **26,** 1710 (2009).
4. Z. Zuo, J. Sun, X. Liu, Q. Jiang, G. Fu, L.-A, Wu, and P. Fu, Phys. Rev. Lett. **97,** 193904 (2006).
5. P.-Z. Z.-Q. Nie, Y.-P. Zhang, T. Jiang, Y.-G. Du, C.-L. Gan, J.-P. Song, and K.-Q. Lu, Chin. Phys. Lett. **24,** 3420 (2007).
6. C.-S. Li, W.-T. Yin, C.-Z. Yuan, M.-Z Shi, Y. Zhao, and Y.-P. Zhang, Chin. Phys. Lett. **27,** 044209 (2010).
7. C. Li, Y. Zhang, Z. Nie, Y. Du, R. Wang, J. Song, and M. Xiao, Phys. Rev. A **81,** 033801 (2010).
8. L. Jia, F. Zhang, M. Li, Y. Liu, and Z. Chen, Chin. Opt. Lett. **7,** 617 (2009).
9. Z. Chu, J. Liu, K. Wang, and J. Yao, Chin. Opt. Lett. **8,** 697 (2010).
10. S. E. Harris, Phys. Today **50,** 36 (1997).
11. H. Ling, Y. Li, and M. Xiao, Phys. Rev. A **53,** 1014 (1996).
12. B. Wang, Y. Han, J. Xiao, X. Yang, C. Xie, H. Wang, and M. Xiao, Opt. Lett. **31,** 3647 (2006).
13. C.-J. Zhu, A.-A. Senin, Z.-H. Lu, J. Gao, Y. Xiao, and J.-G. Eden, Phys. Rev A **72,** 023811 (2005).
14. W. C. Magno, R. B. Prandini, P. Nussenzveig, and S. S. Vianna, Phys. Rev. A **63,** 063406 (2001).